Talanta 81 (2010) 1607–1612

Contents lists available at ScienceDirect

Talanta

journal homepage: www.elsevier.com/locate/talanta

Studies on the sensing behaviour of nanocrystalline $CuGa_2O_4$ towards hydrogen, liquefied petroleum gas and ammonia

Soumya Kanti Biswas, Arpita Sarkar, Amita Pathak, Panchanan Pramanik*

Department of Chemistry, Indian Institute of Technology Kharagpur, Kharagpur 721302, West Bengal, India

ARTICLE INFO

Article history:
Received 26 December 2009
Received in revised form 6 March 2010
Accepted 8 March 2010
Available online 17 March 2010

Keywords:
Chemical synthesis
Nanocrystalline $CuGa_2O_4$
Gas sensor
LPG
H_2
NH_3

ABSTRACT

In the present article, the gas sensing behaviour of nanocrystalline $CuGa_2O_4$ towards H_2, liquefied petroleum gas (LPG) and NH_3 has been reported for the first time. Nanocrystalline powders of $CuGa_2O_4$ having average particle sizes in the range of 30–60 nm have been prepared through thermal decomposition of an aqueous precursor solution comprising copper nitrate, gallium nitrate and triethanol amine (TEA), followed by calcination at 750 °C for 2 h. The synthesized nanocrystalline $CuGa_2O_4$ powders have been characterised through X-ray diffraction (XRD), transmission electron microscopy (TEM), field-emission scanning electron microscopy (FESEM) study, energy dispersive X-ray (EDX) analysis and BET (Brunauer–Emmett–Teller) surface area measurement. The synthesized $CuGa_2O_4$ having spinel structure with specific surface area of 40 m^2/g exhibits maximum sensitivity towards H_2, LPG, and NH_3 at 350 °C.

1. Introduction

Metal oxide semiconductor materials are well-known for the detection of inflammable and toxic gases in air. In fact, high sensitivity, fast response, high chemical and thermal stability, high reliability, low cost, and compacted size have promoted the semiconductor metal oxides to the attractive gas sensor materials, even if they are usually operating at high temperatures [1].

Of the various oxide materials, the transition metal based composite or complex oxides are popular for their enhanced response towards different reducing/oxidizing gases in air. Titanates [2,3], stannates [4–6], niobates [7–10], ferrites [11–14] and tantalates [15] are among those transition metal oxide compositions that have been extensively investigated for their gas sensing behaviours towards different gases. Review of the available literature on gas sensor materials reveals that transition metal gallates with a general formula of AB_2O_4 are among the least investigated oxide systems so far. $ZnGa_2O_4$ [16] and $Cd_{1-x}Mg_xGa_2O_4$ [17] with spinel structures, are the only two metal gallate systems that have been reported for their gas sensing behaviour till date. The present paper aims on this inadequacy and thus, focuses on the synthesis of nanocrystalline $CuGa_2O_4$ powders through a chemical process for the first time, and studies of their response towards different reducing gases such as, H_2, liquefied petroleum gas (LPG), and NH_3.

The sensitivity to gases depends on the microstructure of the sensing material, especially on the porosity and grain size. Nanocrystalline gas sensors materials have received great interest for their improved sensitivity due to high surface-to-volume ratio and thus a great surface activity.

2. Experimental

2.1. Raw materials

(i) Copper nitrate, (ii) gallium metal, (iii) triethanolamine (TEA), (iv) ammonia (25%), and (v) nitric acid (70%). All the materials were procured from M/S Aldrich (USA).

2.2. Preparation of aqueous solution of gallium nitrate

In this study, an aqueous solution of gallium nitrate was prepared in the laboratory from gallium metal and stocked for use as a source of gallium in the synthesis of nanocrystalline powders of $CuGa_2O_4$. The aqueous solution of gallium nitrate was prepared by dissolving weighed amount of metallic gallium in minimum quantity of concentrated nitric acid under control heating followed by addition of required amount of deionised water to make a 0.1 M aqueous solution of gallium nitrate.

* Corresponding author. Tel.: +91 3222 283322; fax: +91 3222 255303.
E-mail addresses: soumyakb@chem.iitkgp.ernet.in (S.K. Biswas), pramanik@chem.iitkgp.ernet.in, panchanan_123@yahoo.com (P. Pramanik).

0039-9140/$ – see front matter © 2010 Elsevier B.V. All rights reserved.
doi:10.1016/j.talanta.2010.03.010

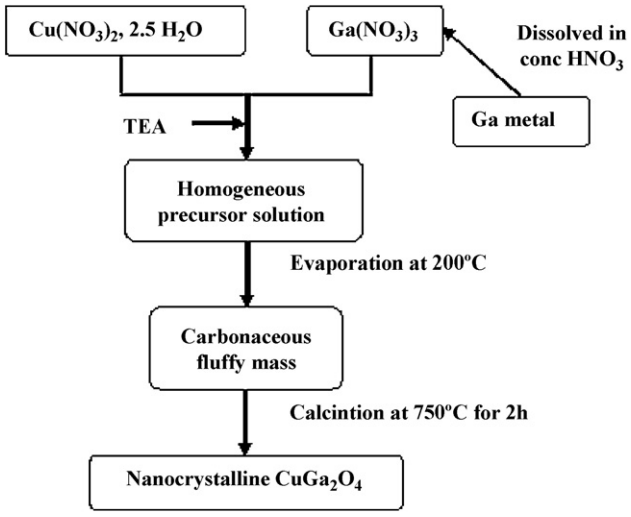

Fig. 1. Schematic representation of the preparation of the nanocrystalline powders of $CuGa_2O_4$.

2.3. Synthesis of nanocrystalline $CuGa_2O_4$ powder with spinel structure by decomposition of aqueous based organic precursor solution

100 ml of aqueous solution of copper nitrate (0.1 M) was mixed with 200 ml of aqueous solution of gallium nitrate (0.1 M), maintaining the molar ratio of Cu^{2+} to Ga^{3+} at 1:2 in the solution mixture. TEA (4 moles per mole of cations present in the solution mixture) was then added into the solution mixture under constant stirring. The pH of the final solution mixture was maintained at almost 6 with the help of ammonia to avoid any undesired precipitation. This solution was then heated at about 200 °C until complete dehydration occurred and metalo-organic complexes underwent oxidative-decomposition with the evolution of dense fumes to generate a voluminous fluffy carbonaceous mass [18]. The black fluffy mass was then crushed into powders. Subsequent calcination of this carbonaceous precursor powders at 750 °C for 2 h produced carbon-free nanocrystalline powders of $CuGa_2O_4$ having spinel structure. The method for the preparation is schematically depicted in Fig. 1.

2.4. Material characterization

The $CuGa_2O_4$ powders calcined at different temperatures ranging from 550 °C to 750 °C for 2 h were characterized through X-ray powder diffraction (XRD) study using an X'Pert-pro diffractometer operated at 40 kV and 25 mA with CoKα radiation and a Ni filter. Measurement was performed at room temperature under vacuum to minimize air scatter. The data were collected over the 2θ angle range of $20^\circ \leq 2\theta \leq 80^\circ$ with a step size of 0.05°. The step time was 2 s. For the phase identification, the obtained XRD pattern was analyzed by comparing with PCPDFWIN [19] data file. The crystallite size (D) of the compositions was calculated using Scherrers equation [20] to the full widths at half maxima (FWHM) of the diffraction peaks and introducing the correction for instrumental broadening with respect to standard silicon. The actual FWHMs were calculated by the following equations considering the peaks to be of the Gaussian type:

$$(\beta^{o})^2 = (\beta^{m})^2 - (\beta^{s})^2; \quad D = \frac{0.9\lambda}{\beta^{o}\cos\theta}$$

where β° = FWHM considering the particle size effect, β^{m} = integral of FWHM, β^{s} = FWHM due to instrumental effect for the standard Si, θ = half incident angle of the X-ray, and λ = wavelength of the target material (λ = 1.7902 Å). The transmission electron microscopy (TEM) studies were carried out with 200 keV electron beams using JEOL 2010 (ultrahigh-resolution model). For the TEM experiment, the samples were prepared by suspending the heat-treated powder in ethyl alcohol by sonication and taking a drop of the suspension on a 200-mesh carbon coated copper grid. The surface morphology was studied using a JEOL-JSM6500 field-emission scanning electron microscope (FESEM) equipped with an energy dispersive X-ray (EDX) analyzer (Oxford). The BET (Brunauer–Emmett–Teller) specific surface areas of the calcined powders (after out-gassing the powders at 200 °C for 4 h) were determined through N_2 adsorption isotherms at 77 K using a Beckman Coulter SA3100 surface area analyzer.

2.5. Electrical measurements and gas sensing studies

Electrical as well as gas sensing properties of the synthesized material were studied by two probes DC conductivity measurements. For the experiment, a pellet (10 mm diameter and 1–2 mm thickness) was made from the powder material using 1–2 drops of poly vinyl alcohol (PVA) (5%). The pellet was then heat-treated at 450 °C for 4 h to remove the residual polymer which helped to produce porous solid. The porous pellet with thin platinum electrodes was housed inside a quartz test-chamber, which was heated by a resistance furnace. The temperature of the test-chamber was controlled using a temperature controller. Resistance of the sensor was measured using autoranging microvolt DMM (Model 197A, M/s Keithley Instruments, USA) for low temperatures (when the resistance is higher than 100 MΩ) and Agilent Data Acquisition/Switch Unit (model no. 34970A) for higher temperatures. At each sensor operating temperature, the test gas was injected into the chamber through an injection port after a steady base line resistance in air was established. The corresponding change of electrical resistance of the material was measured as a function of time till a constant resistance value was achieved. Next, the chamber was purged with dry air for 2–3 min; the steady base line of resistance value was attained and then the next experiment was performed. The response of the material to the test gases was calculated using the following equation:

$$\text{response}\,(\%) = \left[\frac{R_a - R_g}{R_a}\right] \times 100$$

In the above equation, R_a represents the resistance of the pellet in air and R_g the resistance of the same in the presence of a test gas. The response of the material was studied to H_2, liquefied petroleum gas (LPG), and NH_3 in the temperature range of 200–400 °C. There were three tests made for each gas at each operating temperature to confirm the results. The reproducibility of the experiments was checked by repeating the same experiment with two more pellets. Prior to sensor experiments samples were thermally conditioned by annealing in dry air at 300 °C to remove any adsorbed water and allowed equilibrium to be achieved with oxygen through the flow of air. The response value, response time and recovery time of the sensor were determined from the decrease of the resistance in the presence of a reducing gas (i.e. response process) and the regain of the initial value of resistance in air (recovery process) with change of time. Response time is considered as the time required for achieving 90% of final change in conductance after the test gas is injected and recovery time is taken as the time needed for the sensor to attain a conductance 10% above the original value in air.

3. Results and discussion

Phase analysis and structural characterization of the prepared $CuGa_2O_4$ powders were carried out through room temperature XRD studies. Fig. 2 shows the XRD patterns of the carbonaceous

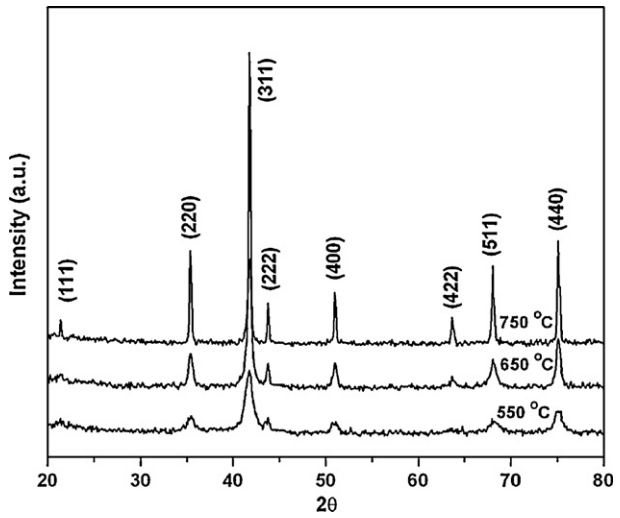

Fig. 2. X-ray diffractogram (using CoKα radiation) of the $CuGa_2O_4$ calcined at 550–750 °C for 2 h.

powders of $CuGa_2O_4$ calcined at different temperatures ranging from 550 °C to 750 °C for 2 h. The onset of crystallization process in the precursor powder sample was noticeable through the incipient peaks in the XRD pattern when the carbonaceous precursor of $CuGa_2O_4$ was calcined at 550 °C for 2 h. Calcination at this low temperature could not completely crystallize the material as indicated by the low intensity diffraction lines in the XRD pattern of the sample on calcination at 550 °C for 2 h. The carbonaceous precursor powders of the sample were calcined at 750 °C for 2 h and a single phase $CuGa_2O_4$ was realized. The absence of any additional diffraction lines in XRD of the powders calcined at 750 °C for 2 h confirmed the formation of a pure spinel phase of $CuGa_2O_4$ as per the standard data reported in JCPDS file (card no. 044-0183) and the diffraction lines were indexed accordingly. Despite the advantages of better chemical homogeneity and low phase formation temperature offered through the chemical synthesis process in comparison to solid-state method, there is no report on the preparation of $CuGa_2O_4$ through wet chemical method in literature. The calculated lattice parameters [$a = b = c = 8.292$ Å and $\alpha = \beta = \gamma = 90°$] of the sample matched closely with the standard lattice parameter values (8.3 Å; JCPDS card no. 044-0183). The average crystallite size of the synthesized powders evaluated from line broadening analysis using a Scherrers formula was found to be 30 nm.

The chemical composition of the calcined powders at 750 °C was analyzed using EDX (Fig. 3), which confirmed the expected chemical composition of $CuGa_2O_4$ with the observed stoichiometric ratio of Cu:Ga in the compound of 1:2.

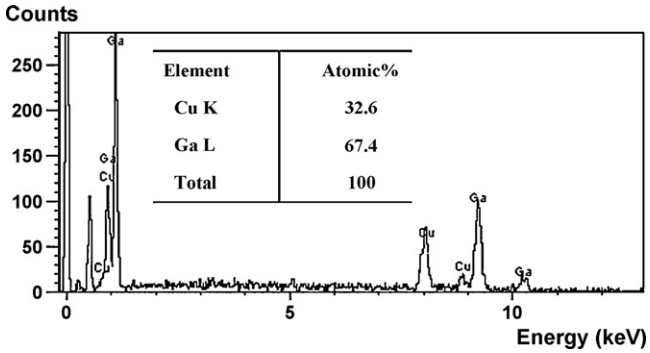

Fig. 3. EDX analysis of the $CuGa_2O_4$ after calcination at 750 °C for 2 h.

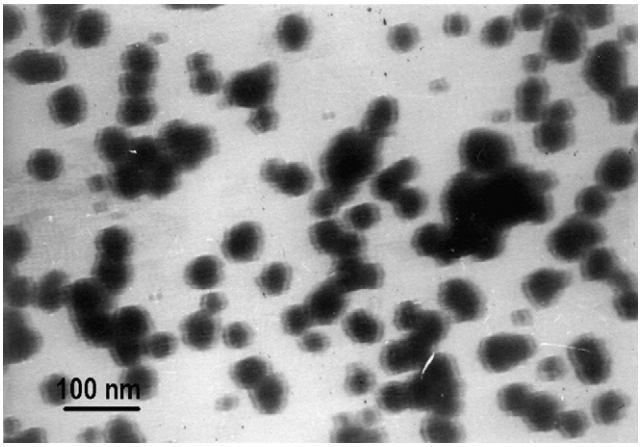

Fig. 4. Bright field TEM micrograph of the calcined (at 750 °C for 2 h) $CuGa_2O_4$.

The microstructure of the calcined powders of $CuGa_2O_4$ was observed through TEM studies. Fig. 4 shows the bright field electron micrograph of the synthesized $CuGa_2O_4$. The particles visible in the micrograph can be identified as nanoparticles with size in the range of 30–60 nm. The micrograph showed that the particles were nearly monodisperse and the particle sizes were comparable with the average crystallite size calculated from XRD data using Scherrers equation.

FESEM experiments were carried out using both, the calcined powders of $CuGa_2O_4$ and porous pellet of the calcined $CuGa_2O_4$ powders. Fig. 5 is a FESEM image of the calcined powders of $CuGa_2O_4$ showing morphology of the nanocrystalline particles. The low processing temperature involved in this method prevented hard agglomerations in the powder as seen from the FESEM image (Fig. 5). The micrograph revealed that powders were dominated by the approximately spherical particles with distinct grain boundaries that were uniformly distributed with the size in the range of 30–60 nm.

FESEM micrograph of the porous pellets derived from calcined $CuGa_2O_4$ nanocrystalline powders (Fig. 6) provided information of the microstructure and topology of the pellet surface. The micrograph clearly showed the porous nature of the surface of the pellets and also indicated that the compression of the powder on pelletisation resulted in agglomerations in some portions of the surface of the pellets.

Electrical conduction in metal oxides is thermally activated process. The variation of electrical conductivity of $CuGa_2O_4$ pellets was measured as a function of temperature in dry air in the

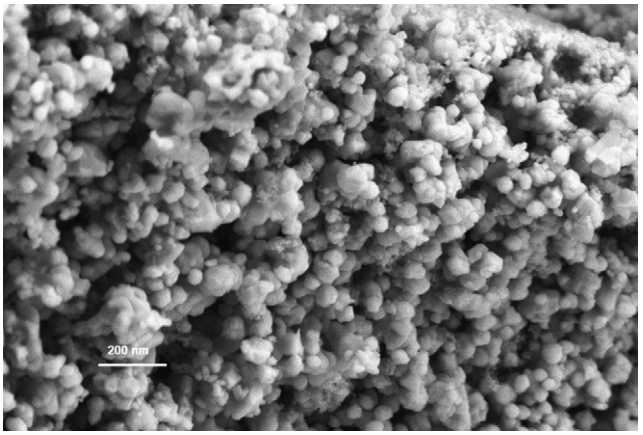

Fig. 5. FESEM image of the calcined (at 750 °C for 2 h) $CuGa_2O_4$ powders.

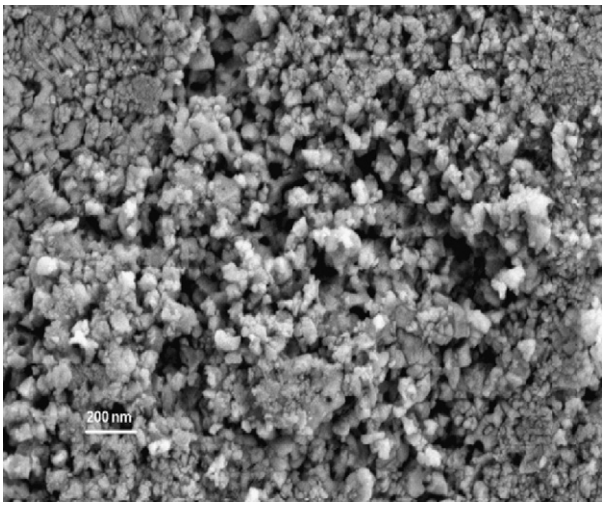

Fig. 6. FESEM image of pellet surface derived from nanocrystalline powders of $CuGa_2O_4$.

temperature range of 200–400 °C. Fig. 7 depicts the *dc* electrical conductivity–temperature behaviour of the pellet of $CuGa_2O_4$ in air which corresponded to Arrhenius-type plots. In the whole temperature range of 200–400 °C, the logarithm of conductivity of the material changed almost linearly with the reciprocal temperature ($1/T$) as expected for a typical semiconducting material with no hysteresis during heating and cooling cycles. The activation energy (E_a) determined in terms of the slope of the Arrhenius plot was found to be 0.47 eV in air. The material showed typical *n*-type conductivity behaviour since its electrical resistance decreased in the presence of reducing gases and the resistance increased when exposed to O_2.

Figs. 8–11 demonstrate the typical temperature dependence of response of compressed powder of $CuGa_2O_4$ (sintered at 450 °C for 4 h) towards 500 ppm of H_2, LPG, and NH_3 respectively. The pellets made of nanocrystalline powders of $CuGa_2O_4$ showed the maximum responses towards H_2, LPG, and NH_3 at 350 °C. For 500 ppm H_2, the maximum response of 82% was observed at 350 °C for the pellets of $CuGa_2O_4$. The response was found to decrease to 66% at 400 °C. For 500 ppm LPG, the observed maximum response was found to be around 72% at 350 °C. The response (towards LPG) was observed to decrease to 61% at 400 °C. The maximum response towards 500 ppm NH_3 observed at 350 °C was 37%.

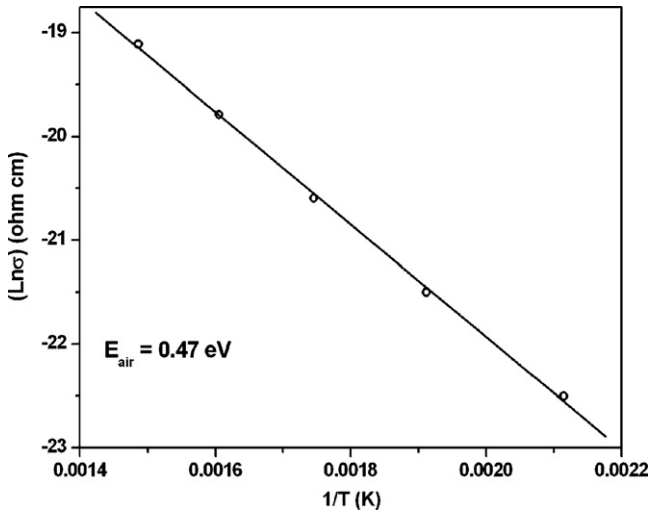

Fig. 7. Arrhenius plot for electrical conductivity of $CuGa_2O_4$ in air.

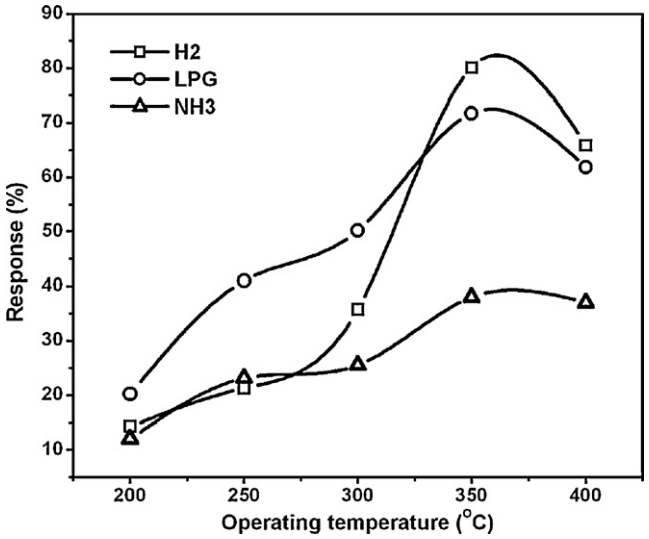

Fig. 8. Response characteristics of nanocrystalline $CuGa_2O_4$ in the form of porous pellet towards 500 ppm each of H_2, LPG, and NH_3 in air as a function of temperature.

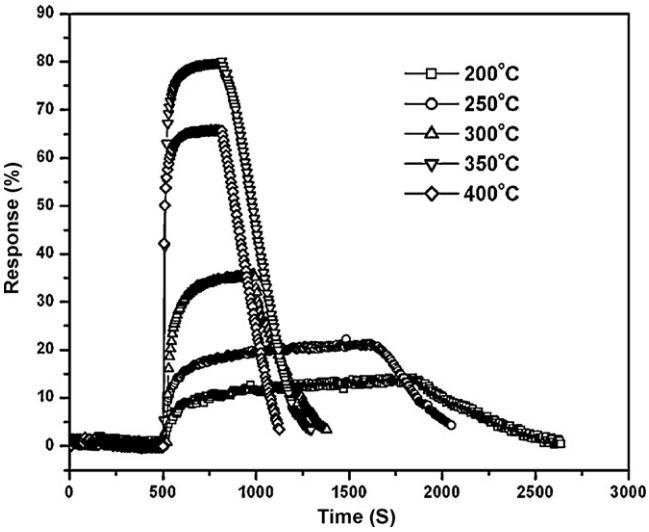

Fig. 9. Responses of porous pellet of nanocrystalline $CuGa_2O_4$ towards 500 ppm of H_2 in air at different temperatures.

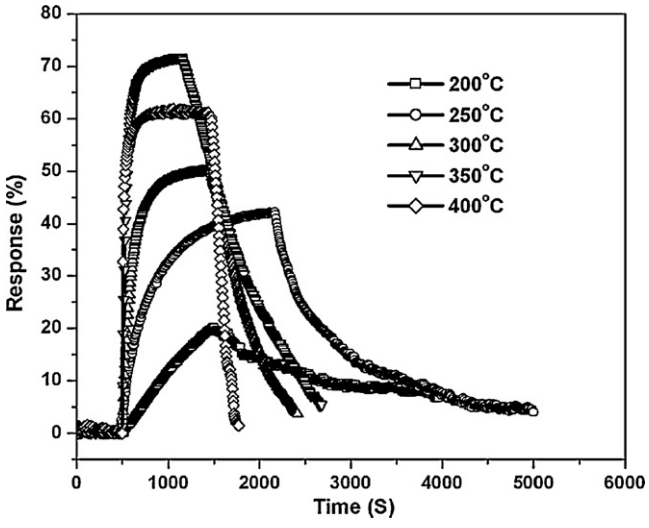

Fig. 10. Responses of porous pellet of nanocrystalline $CuGa_2O_4$ towards 500 ppm of LPG in air at different temperatures.

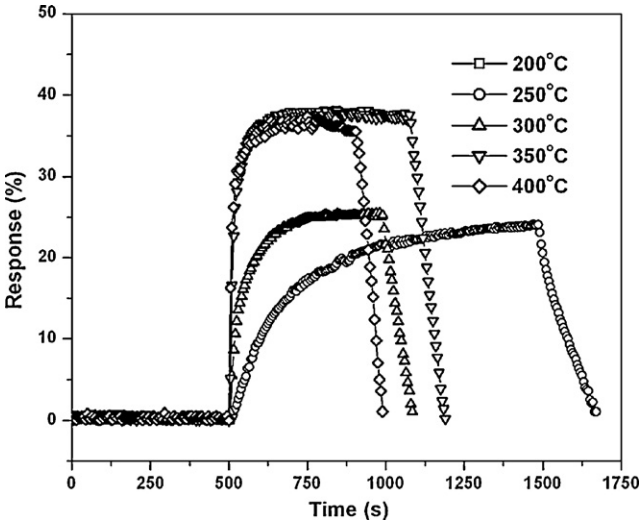

Fig. 11. Responses of porous pellet of nanocrystalline $CuGa_2O_4$ towards 500 ppm of NH_3 in air at different temperatures.

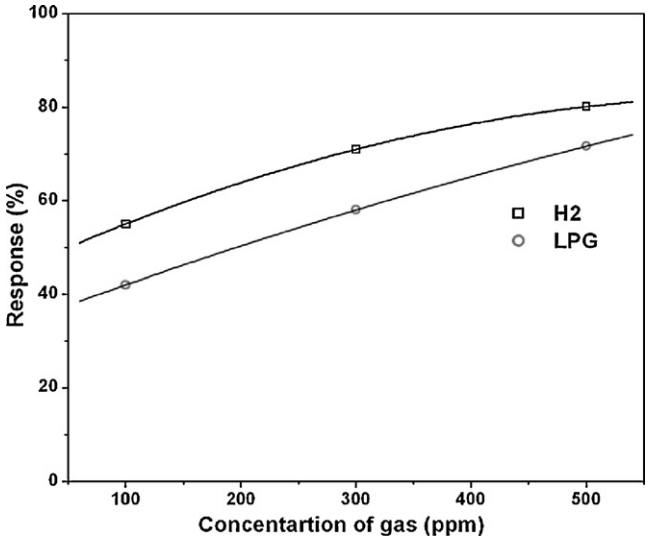

Fig. 13. Variation of response of porous pellet of nanocrystalline $CuGa_2O_4$ with concentration of H_2 and LPG at 350 °C.

There were three tests made for each gas at each operating temperature to confirm the results. Fig. 12 represents three cycles of response–recovery characteristics of the material exposed to 500 ppm LPG at 350 °C.

For high responses towards H_2 and LPG at 350 °C, this temperature was selected for calibration experiments at different concentrations of test gases. Fig. 13 shows the responses towards H_2 and LPG of different concentrations (100, 300 and 500 ppm) at 350 °C which were found to increase almost linearly with gas concentrations.

Typical response and recovery characteristics of $CuGa_2O_4$ pellets operating at different temperatures towards 500 ppm of gases are shown in Fig. 14. The response and recovery time (at the temperature when maximum response was achieved) for the pellets of $CuGa_2O_4$ towards H_2 were found to be around 120 and 460 s respectively (at 350 °C), and towards LPG, they are 305 and 1110 s respectively (at 350 °C), while towards NH_3 the respective values were 105 and 140 s (at 350 °C).

The response was found to decrease at higher operating temperatures as can be seen in Figs. 8–11. This behaviour can be explained by considering the increase of desorption on the surface of the sensor materials at higher temperature. Besides this, the increase of the charge carrier concentration and the decrease of the Debye length of the semiconductor material at higher temperature may be responsible for the decrease in the response at higher temperatures [9,10].

The gas sensing phenomenon involves the change of electrical resistance of the sensor material in the presence of gases due to the oxidation of the reducing gases by the surface chemisorbed oxygen species (like O^-, O^{2-}, O_2^-, etc.), which releases the electrons and thus increases the charge in the conduction band of the *n*-type oxide and hence the conductivity gets increased (i.e. decrease of the potential barrier). The extent of adsorbed oxygen ions and existence of their different chemical forms (O^-, O^{2-}, O_2^-, etc.) on the sensor surface are controlled by the sensor operating temperature:

$$O_{2(g)} + e^- \rightarrow O_{2(ads)}^-$$

$$O_{2(ads)}^- + e^- \rightarrow 2O_{(ads)}^-$$

The oxidation reactions of H_2 and LPG could be represented as follows [9,10]:

$$C_pH_{2p+2} + (3p+1)O_{(ads)}^- \rightarrow pCO_2 + (p+1)H_2O_{(g)} + (3p+1)e^-$$

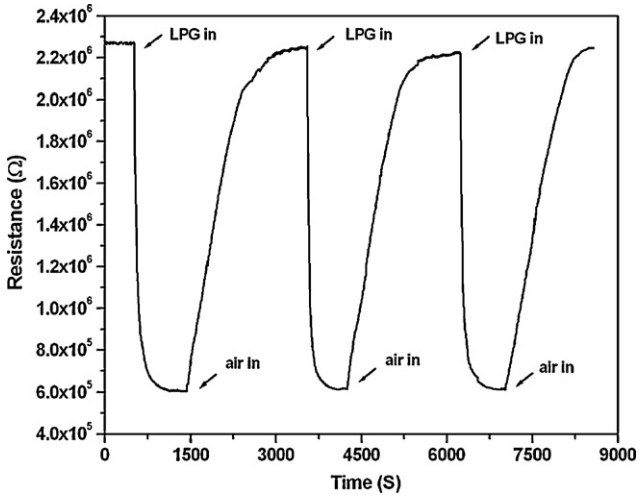

Fig. 12. Electrical resistance of porous pellet of $CuGa_2O_4$ in alternating environments of air and 500 ppm LPG at 350 °C.

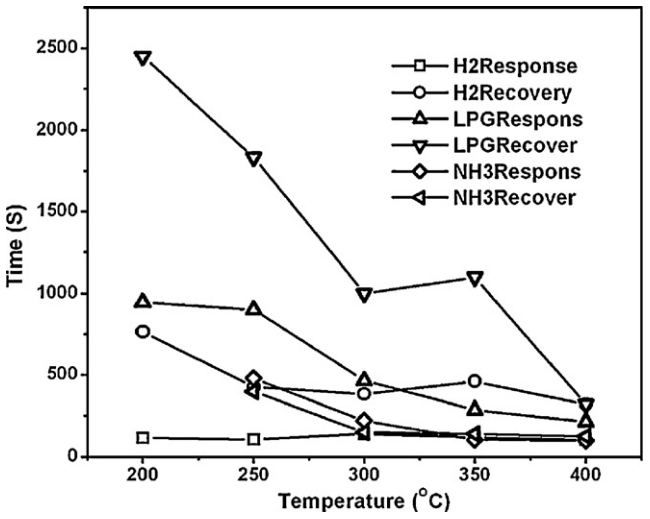

Fig. 14. Temperature variation of response time and recovery time for $CuGa_2O_4$ for 500 ppm H_2, LPG and NH_3.

LPG is a mixture of hydrocarbons like *n*-propane and *n*-butane, so $p = 3$ or 4. This equation is valid for H_2 when $p = 0$.

The oxidation reactions of NH_3 could be represented as follows [9,10]:

$$2NH_3 + 3O_{(ads)}{}^- \rightarrow N_2 + 3H_2O + 3e^-$$

4. Conclusion

Nanocrystalline $CuGa_2O_4$ powders have been synthesized by aqueous based metal ion-ligand complex precursor route for the first time. The spinel structure of $CuGa_2O_4$ was realized at 750 °C. The low processing temperature in this method prevented grain growth in the powder. TEM images showed the average particle sizes in the range of 30–60 nm and specific surface area of 40 m^2/g. The n-*type* semiconducting nanocrystalline $CuGa_2O_4$ showed the sensitivities towards H_2, LPG and NH_3. The maximum responses of $CuGa_2O_4$ towards H_2, LPG and NH_3 were found to be around 82%, 72%, and 37% at 350 °C respectively.

References

[1] B. Bott, T.A. Jones, B. Mann, Sens. Actuators 5 (1984) 65.
[2] J. Gerblinger, U. Lampe, H. Meixner, V. Perczel, J. Giber, Sens. Actuators B: Chem. 18–19 (1994) 529.
[3] X. Chu, X. Liu, G. Wang, G. Meng, Mater. Res. Bull. 34 (1999) 1789.
[4] V. Jayaraman, G. Mangamma, T. Gnanasekaran, G. Periaswami, Solid State Ionics 86–88 (1996) 1111.
[5] S. Tao, F. Gao, X. Liu, O.T. Sørensen, Sens. Actuators B: Chem. 71 (2000) 223.
[6] J.W. Fergus, Sens. Actuators B: Chem. 123 (2007) 1169.
[7] D.H. Dawson, D.E. Williams, J. Mater. Chem. 6 (1996) 409.
[8] K.I. Gnanasekar, V. Jayaraman, E. Prabhu, T. Gnanasekaran, G. Periaswami, Sens. Actuators B: Chem. 55 (1999) 170.
[9] S.K. Biswas, T. Gnanasekaran, T.K. Ghorai, P. Pramanik, J. Electrochem. Soc. 155 (2008) J26.
[10] S.K. Biswas, P. Pramanik, Sens. Actuators B: Chem. 133 (2008) 449.
[11] Y.-L. Liu, Z.-M. Liu, Y. Yang, H.-F. Yang, G.-L. Shen, R.-Q. Yu, Sens. Actuators B: Chem. 107 (2005) 600.
[12] P.Y. Lee, K. Ishizaka, H. Suematsu, W. Jiang, K. Yatsui, J. Nanopart. Res. 8 (2006) 29.
[13] B. Baruwati, R.K. Rana, S.V. Manorama, J. Appl. Phys. 101 (2007) 0143021.
[14] Z. Sun, L. Liu, D.Z. Jia, W. Pan, Sens. Actuators B: Chem. 125 (2007) 144.
[15] P.T. Moseley, D.E. Williams, J.O.W. Norris, B.C. Tofield, Sens. Actuators 14 (1988) 79.
[16] L. Satyanarayana, C.V.G. Reddy, S.V. Manorama, V.J. Rao, Sens. Actuators B: Chem. 46 (1998) 1.
[17] J. Wen, X. Ge, X. Liu, Sens. Actuators B: Chem. 115 (2006) 622.
[18] S.K. Biswas, D. Dhak, A. Pathak, P. Pramanik, Mater. Res. Bull. 43 (2008) 665.
[19] PCPDFWIN Version 2.02, May 1999, Copyright 1999 JCPDS-ICDD.
[20] H.P. Klug, L.E. Alexander, X-ray Diffraction Procedures for Polycrystalline and Amorphous Materials, Wiley and Sons, New York, 1974.